


Article

Enhancing Lubrication Performance of Calcium Sulfonate Complex Grease Dispersed with Two-Dimensional MoS₂ Nanosheets

Shuo Xiang ¹ , Xufei Long ², Qinhui Zhang ^{1,*}, Pengfei Ma ¹, Xin Yang ¹, Hui Xu ³, Peng Lu ⁴, Peng Su ¹, Weihua Yang ¹ and Yan He ¹

¹ Army Logistics Academy of PLA, Chongqing 401311, China; xslaplace@163.com (S.X.)

² Unit 32358, Lhasa 850032, China

³ Shandong Honsing Chemical Co., Ltd., Dongying 257335, China

⁴ Unit 91967, Xingtai 054000, China

* Correspondence: 15223276757@163.com

Abstract: Calcium sulfonate complex greases (CSCG) have proven to be a sustainable alternative to lithium complex greases, which still require appropriate additives to deliver lubrication performance benefits under extreme working conditions such as heavy load, high speed, and high temperature. The anti-wear and friction reducing properties of CSCG enhanced by two-dimensional MoS₂ nanosheets (2D MoS₂) with a narrow lateral size and thickness distributions were evaluated by a four-ball tribometer. The results showed that the CSCG with 0.6 wt.% 2D MoS₂ performs best, with a 56.4% decrease in average friction coefficient (AFC), 16.5% reduction in wear scar diameter (WSD), 14.3% decrease in surface roughness, and a 59.4% reduction in average wear depth. Combining SEM-EDS images, Raman, and X-ray photoelectron spectra, it is illustrated that the physical transferred film and tribo-chemical film consisting of MoS₂, Fe₂O₃, FeSO₄, CaCO₃, CaO, and MoO₃ were generated on the worn surface, which improves the lubrication performance of CSCG considerably.

Keywords: two-dimensional MoS₂ nanosheets; calcium sulfonate complex grease; lubrication performance; physical transferred film; tribo-chemical film



Citation: Xiang, S.; Long, X.; Zhang, Q.; Ma, P.; Yang, X.; Xu, H.; Lu, P.; Su, P.; Yang, W.; He, Y. Enhancing Lubrication Performance of Calcium Sulfonate Complex Grease Dispersed with Two-Dimensional MoS₂ Nanosheets. *Lubricants* **2023**, *11*, 336. <https://doi.org/10.3390/lubricants11080336>

Received: 10 July 2023

Revised: 4 August 2023

Accepted: 4 August 2023

Published: 8 August 2023



Copyright: © 2023 by the authors. Licensee MDPI, Basel, Switzerland. This article is an open access article distributed under the terms and conditions of the Creative Commons Attribution (CC BY) license (<https://creativecommons.org/licenses/by/4.0/>).

1. Introduction

Lithium grease is a kind of widely used and multipurpose grease, well known for its outstanding durability, high viscosity, and mechanical stability, which could provide active and enduring protection against oxidization, rust, extreme temperatures, and severe wear. Lithium lubricating greases are also characterized by their wonderful lubrication, excellent water resistance, heavy load bearing, and heat resistance. They are by far the most popular grease across the globe today, and make up more than 75% of lubricating greases across all industries worldwide [1]. Lithium is one of the pivotal components in smartphones and electric vehicle (EV) batteries, but global supplies are under huge strain because of emerging EV demand, which results in lithium prices continuing to escalate drastically [2]. As the industrial and automotive markets continue to evolve, discovering lithium grease alternatives is an urgent subject to be studied. Calcium sulfonate complex greases (CSCG) are manufactured by converting a fluid detergent that contains synthetic calcium sulfonate based on amorphous calcium carbonate to greases formulated with calcite particles, which show exceptional extreme pressure and anti-wear performance, excellent water washout, corrosion prevention, high temperature resistance, good mechanical and shear stability, and low pumpability [3–5]. Even more importantly, they do not need any additives to meet certain requirements, as lithium greases do. Given their excellent properties, performance, and economic viability, calcium sulphonate complex greases are a compelling and sustainable alternative to lithium complex greases.

Conventional lubricant additives, such as molybdenum dialkyl dithiocarbamate (MoDTC), zinc dithiophosphate (ZDTP), and zinc dialkyldithiophosphates (ZDDP) are organic phosphorus compounds, organic sulfide, and organic metal compounds, respectively, and are dissolved or suspended as solids in grease that typically range between 1 and 3 percent of the grease volume [6]. The comparatively small proportion that lubricant additives occupy in greases is an indicator of the power these compounds or complexes afford to lubricating greases. The emergence of two-dimensional materials (2D materials) like transition metal dichalcogenides (TMD) [7–9], graphene [10–12], 2D carbide/nitride [13–15], black phosphorus (BP) [16–18], and SiP [19] as lubricant additives open up new opportunities in promoting the anti-wear and friction reducing properties of mechanical systems across a variety of industries, including construction machinery, mining equipment, steel milling machines, automotive machinery, marine engineering equipment, aeronautical equipment, and farm machines. Two-dimensional materials with a layered structure not only exhibit better performance in the field of friction-reducing and anti-wear behavior, but also result in fewer eco-unfriendly emissions and markedly reduce toxicity more than organic additives, presenting a new paradigm as promising alternatives to traditional lubrication approaches [20].

The synthesis methods of 2D materials can commonly be classified into either top-down techniques, which exfoliate the 2D materials from a raw bulk material, or bottom-up techniques, which see the acceptable 2D materials grown to specification [21]. Representative top-down techniques include mechanical exfoliation, liquid-phase exfoliation, and ion intercalation, while the bottom-up techniques include chemical vapor deposition (CVD), hydrothermal synthesis, and pulsed laser deposition (PLD) [22,23]. Liquid-phase exfoliation is a universal technique for yielding liquid suspensions containing plenty of 2D nanomaterials. This method has been utilized to exfoliate a broad range of materials including graphene, BN, and transition metal dichalcogenides such as MoS₂ and WSe₂, as well as MoO₃, GaS, black phosphorus, and MXenes [24,25]. However, 2D materials fabricated by using liquid-phase exfoliation tend to have a very broad lateral size and thickness distributions, which are complicated as some applications require controlled nanosheet sizes: small nanosheets are ideal for catalysis, whereas large ones are requisite for mechanical reinforcement.

In the present article, 2D MoS₂ with a narrow lateral size and thickness distributions was produced via a liquid-phase exfoliation method, based on liquid cascade centrifugation. The anti-wear and friction-reducing properties of the as-synthesized 2D MoS₂ in CSCG were systematically investigated by a four-ball tribometer. Optical microscopy (OM) and white light interferometer (WLI) methods were applied to characterize the wear surface. The composition and microstructure of the physical adsorption film and tribo-chemical film were analyzed by Raman spectrometry (Raman), scanning electron microscope, energy dispersion spectrum (SEM-EDS), and X-ray photoelectron spectroscopy (XPS). The lubrication mechanism of CSCG enhanced with 2D MoS₂ was studied.

2. Materials and Methods

2.1. Materials

As mentioned in our preceding literature, 2D MoS₂ were produced by a sonication-assisted liquid phase exfoliation method based on liquid cascade centrifugation and a freeze-drying method [26]. Synthetic PAO40 (polyalpha-olefin 40) was commercially obtained from the Shanghai Naco Lubrication Technology Co., Ltd. (Shanghai, China). Overbased calcium petroleum sulfonate (T106D) was acquired from the Liaoning Jiazhi Chemical Co., Ltd. (Liaoyang, China). The 12-hydroxystearate, acetic acid, boric acid, and calcium hydroxide were purchased from the Chuandong Chemical Co., Ltd. (Chongqing, China). GCr15 bearing steel balls made of GCr15 bearing steel with a diameter of 12.7 mm and an HRC59-61 were purchased from the SINOPEC Research Institute of Petroleum Processing Co., Ltd. (Beijing, China). GCr15 bearing steel is one of the most widely used Chinese bearing steels, and is equivalent to US AISI SAE ASTM, European EN, Germany

DIN, Japanese JIS, British BSI, France NF, and ISO standard, and the proportions of its main elements proportion are as follows: C (0.95~1.05 wt.%), Cr (1.40~1.65 wt.%), Cu (<0.25 wt.%), Mn (0.25~0.45 wt.%), Mo (<0.10 wt.%), Ni (<0.30 wt.%), P (<0.25 wt.%), S (<0.025 wt.%), Si (0.15~0.35 wt.%). All above-mentioned chemical reagents were of analytical grade and did not have to be purified further.

2.2. Preparation and Characterization of Calcium Sulfonate Complex Grease with 2D MoS₂

The preparation method of the CSCG is as follows. First, T106D was poured into a certain amount of PAO40 in the vessel and was agitated and heated, and a certain amount of acetic acid, serving as a promoter, was poured into the above mixture. Secondly, when the Newtonian ultrabasic calcium sulfonate was thoroughly converted to a non-Newtonian ultrabasic calcium sulfonate, a certain amount of 12-hydroxystearic acid was poured into it. Thirdly, when the 12-hydroxystearic acid was totally dissolved, calcium hydroxide and boric acid aqueous solutions were poured into the mixed solution to allow the saponification reaction to proceed at 110 °C for 2 h. Fourth, the mixed solution was heated to 130 °C to evaporate the water present after the saponification reaction. Fifth, the mixed solution was gradually and slowly heated to 190 °C for refining and the 2D MoS₂ of specified mass (0, 0.2, 0.4, 0.6, 0.8, and 1.0 wt.%, respectively) were added to the mixed solution, and then they were naturally cooled to room temperature. Finally, the mixtures were ground three times with a three-roll mill to obtain the corresponding grease samples, which were abbreviated as CSCG, CSCG + 0.2 wt.% 2D MoS₂, CSCG + 0.4 wt.% 2D MoS₂, CSCG + 0.6 wt.% 2D MoS₂, CSCG + 0.8 wt.% 2D MoS₂, and CSCG + 1.0 wt.% 2D MoS₂. Images of all prepared grease samples are presented in Figure 1.

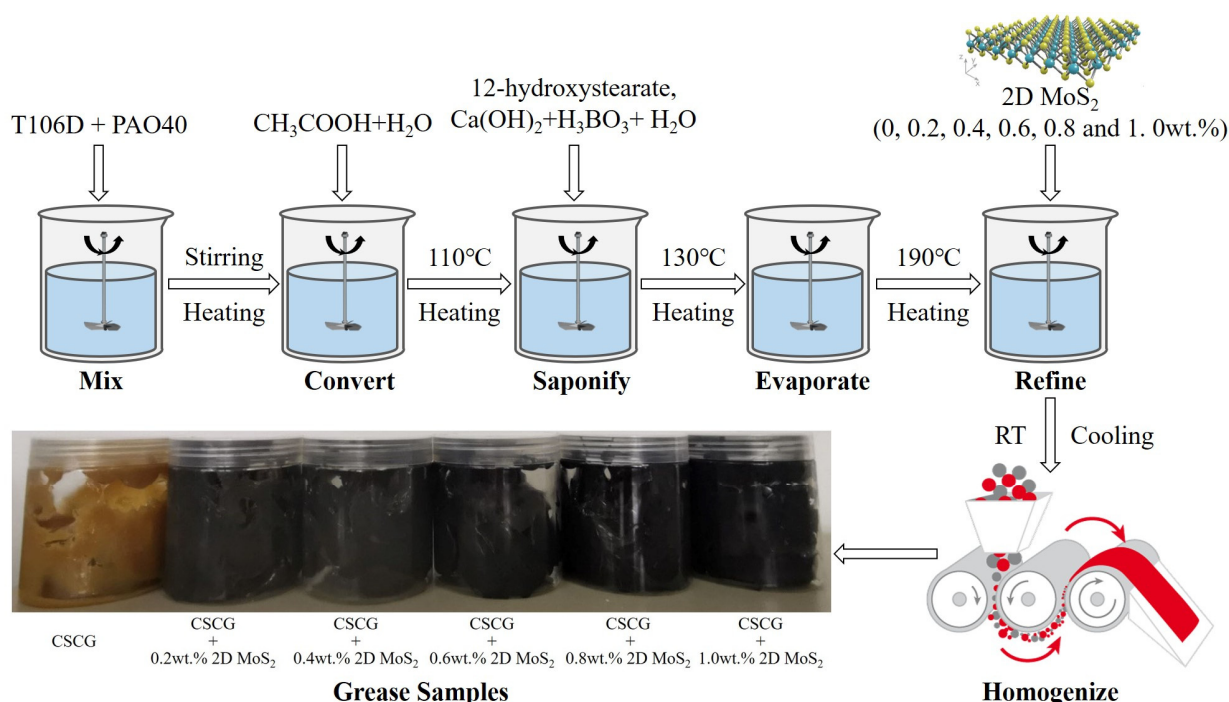


Figure 1. Images of CSCG with various concentrations of 2D MoS₂.

The penetration, dropping point, oil separation, and evaporation loss of the produced greases were measured according to the GB/T 269, GB/T 3498, NB/SH/T 0324, and GB/T 7325 standards, which are similar to the ASTM D217, ASTM D2265, ASTM D6184, and ASTM D972, respectively.

2.3. Tribology Tests and Analysis

The anti-wear and friction-reducing properties of six grease samples are measured by the four-ball tester according to GB/T 3142 (equivalent to ASTM D2783), and test conditions

are 392 N, 1200 rpm, 60 min, 75 °C. First of all, insert one of the washed steel balls into the ball chuck and then insert the ball chuck into spindle of the tester and tighten carefully. Secondly, place the right amount of the grease into the oil cup to fill the void space between the three washed steel balls and the bottom of the oil cup and then lock the balls in position by hand tightening. Thirdly, coat the four test balls and oil cup completely and thoroughly with the test grease samples and then place the oil cup assembly containing the three test steel balls. Fourthly, after the desired test load (392 N) and temperature (75 °C) are reached, start the timer and the drive motor (previously set to 1200 ± 60 rpm) synchronously. Finally, after the drive motor has been operated for 60 ± 1 min, turn off the heaters and drive motor and remove the oil cup assembly. Wash both the steel balls and oil cup ultrasonically with petroleum ether and then remove the solvent using an electric hair dryer before and after testing. The friction coefficient (COF) was automatically recorded by the computer and the wear scar diameter (WSD) on the three lower balls was measured by optical microscope. To guarantee the repeatability and accuracy of the results, three tests were carried out under the same conditions, and the average value was obtained.

After the tribology test, the morphology of worn surfaces was determined by scanning electron microscopy (SEM) with a JEOL JSM-6610LV scanning electron microscope and white light interferometer (WLI) with the ContourGT-X 3D Optical Profiler, and the elemental distribution over the worn surfaces was determined by an Oxford X-Max 20 mm² energy-dispersive X-ray spectrometer. The Raman spectra of worn surfaces were measured using Raman spectrometry (LabRAM HR Evolution, HORIBA, Longjumeau France) with a laser wavelength of 532 nm. X-ray photoelectron spectroscopy (XPS) spectra were tested on an ESCALAB 250Xi X-ray photoelectron spectrometer for probing tribo-film deposition.

3. Results and Discussion

3.1. Physico-Chemical Properties

The most important feature of a grease is its consistency. A grease must be neither too soft nor too stiff, which may result in migrating away from the lubrication area that needs to be lubricated or feeding into the area requiring lubrication with difficulty. The grease consistency depends primarily on the kind and amount of thickener used and the viscosity of the base oil. The measurement of consistency for grease is its resistance to deformation caused by an applied force, which is called penetration. Dropping point is the temperature at which a drop of grease material starts to melt or drip while heated under a prescribed ramped temperature program. The measurement of dropping point for grease is its heat resistance, which indicates the upper temperature limit at which a grease retains its structure, not the maximum operating temperature at which a grease may be used. Greases gradually release oil onto the contact areas of the rubbing surfaces in order to lubricate them and the amount of oil separation depends upon the thickener type, temperature, base oil, and manufacturing method. Some amount of oil releasing from a grease is both normal and necessary to provide lubrication to the intended application. The measurement of oil separation is its tendency to separate oil during storage when stored at room temperature, subjected to high centrifugal forces, or under pressure. Evaporation loss is the determination of the loss of volatile materials from grease or oil, which may bring about thickening or hardening of the grease. The 1/4 penetration, dropping point, oil separation, and evaporation of the 2D MoS₂ nanosheet-containing CSCG are listed in Figure 2. Upon increasing the 2D MoS₂ content in CSCG, the dropping points and oil separation values decreased first and then increased while the evaporation losses decreased as compared with the CSCG. The 2D MoS₂ present in CSCG could effectively improve the holding ability of sulfonate calcium and complex calcium soap fiber networks for mineral oil due to its high adsorption capacity [27]. The penetration of grease samples increases at first, then decreases. This means that the addition of 2D MoS₂ can improve the consistency of grease samples to a certain extent, indicating that 2D MoS₂ had an obvious thickening effect on the CSCG due to its large specific surface area and good dispersity.

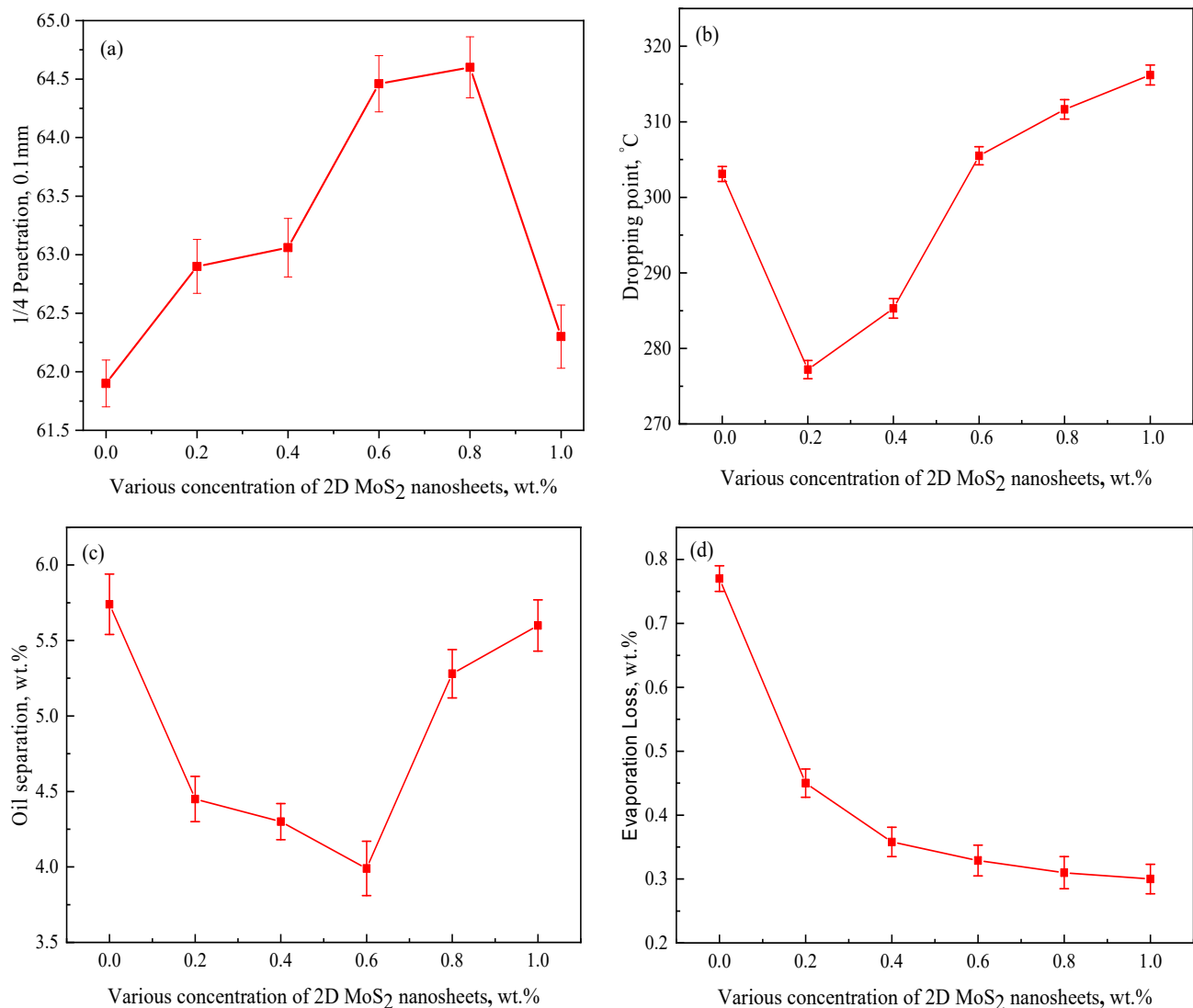


Figure 2. Effect of 2D MoS₂ on (a) penetration, (b) dropping point, (c) oil separation, and (d) evaporation loss of CSCG.

3.2. Lubrication Performance

Lubricating grease is a balanced mixture of base oil, thickener, and performance additives. The base oil and additives are the dominating components in grease formulation and, as such, exert crucial influence on the anti-wear and friction-reducing properties of the grease, while the thickener transforms base oil into the solid to semifluid product. A lower COF produces less friction, which means a better friction reducing property. A larger WSD indicates a poor anti-wear property while a smaller one indicates an outstanding anti-wear property. Figure 3 displays the variations of the COF and the average friction coefficient (AFC) lubricated by CSCG with additive concentrations of 2D MoS₂. From Figure 3a, the friction curve of CSCG tended to stabilize promptly after the peak, while the friction curves were always in a variable state after adding 2D MoS₂, except when the concentration of 2D MoS₂ was 0.6 wt.%. As it can be seen in Figure 3b, the AFC decreases at first and then increases with increase in the concentration of 2D MoS₂. Compared with CSCG, the CSCG + 0.6 wt.% 2D MoS₂ shows the lowest AFC, which was 0.041, reducing by 56.4%. Moreover, all the greases with 2D MoS₂ show smaller AFC than that of CSCG, proving that 2D MoS₂ can effectively improve the antifriction performance.

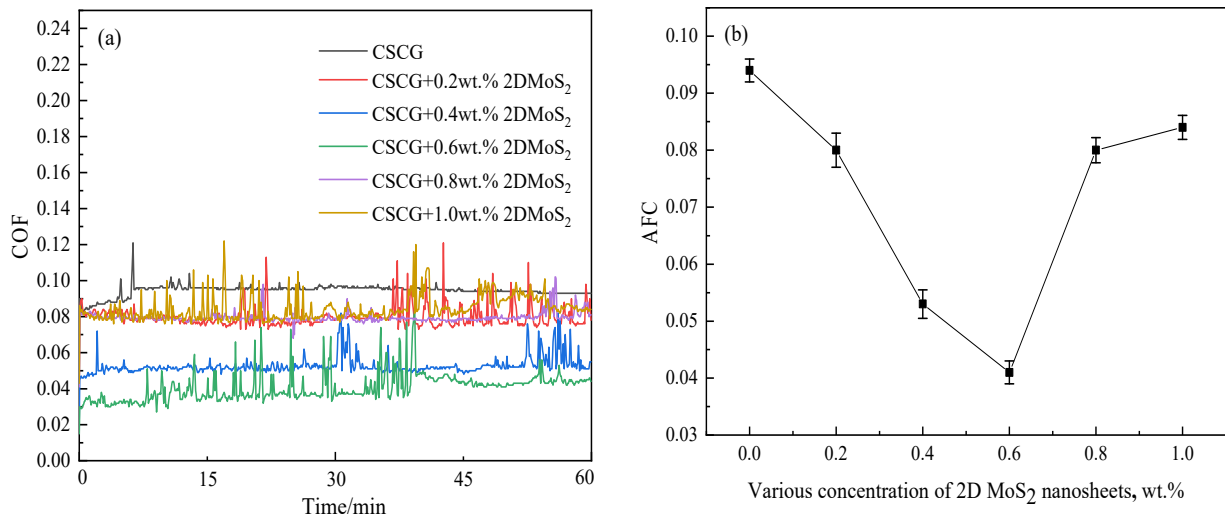


Figure 3. T Variations of COF and AFC with concentration of 2D MoS₂ (a) COF, (b) AFC (1200 rpm, 392 N, 60 min, 75 °C).

After each four-ball test, the three lower steel balls were fetched out for wear scar measurement. Figure 4 shows that the WSD of the steel balls decreases step by step from 0.474 mm to 0.396 mm as the concentrations of 2D MoS₂ grows from 0 to 0.60 wt.%. A further 2D MoS₂ increase leads to an increase in WSD up to 0.447 mm at 1.0 wt.% 2D MoS₂. Compared to CSCG, the smallest WSD of 0.396 mm is measured for a 2D MoS₂ content of 0.6 wt.%, reducing by 16.5%. It was indicated that there was an optimum value for the 2D MoS₂ concentration, and CSCG had the best anti-wear effect when it was 0.6 wt.%.

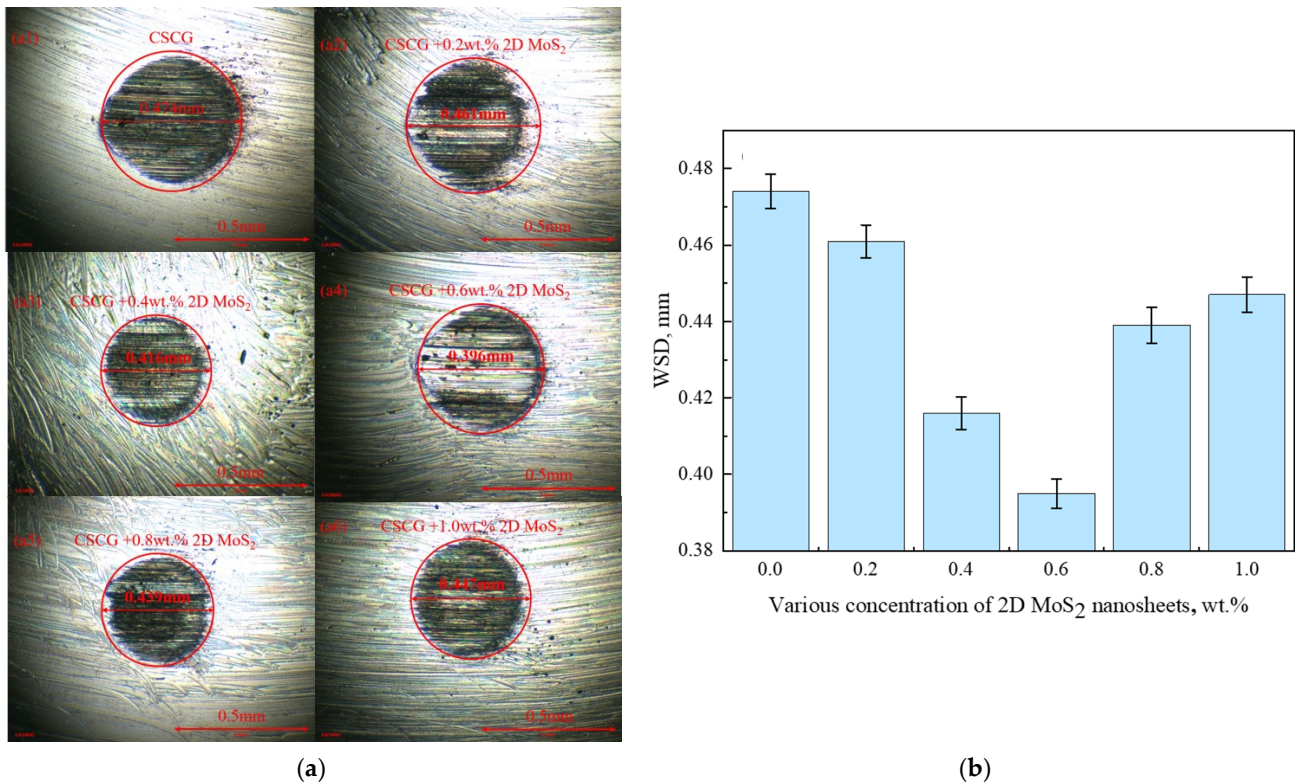


Figure 4. Variations of WSD with concentration of 2D MoS₂: (a) optical micrographs of worn surface on steel ball (a1–a6 lubricated by CSCG, CSCG + 0.2 wt.% 2D MoS₂, CSCG + 0.4 wt.% 2D MoS₂, CSCG + 0.6 wt.% 2D MoS₂, CSCG + 0.8 wt.% 2D MoS₂, and CSCG + 1.0 wt.% 2D MoS₂, respectively), (b) WSD (1200 rpm, 392 N, 60 min, 75 °C).

This test was conducted for the purpose of obtaining the visual and intuitive evidence of the anti-wear property of CSCG before and after it was improved by 2D MoS₂ under the test conditions of 392 N, 1200 rpm, 60 min, 75 °C. Figure 5 displays the 3D morphology of the steel ball wear scar surface lubricated by CSCG and CSCG + 0.6 wt.% 2D MoS₂. Although the morphologies for CSCG and CSCG + 0.6 wt.% 2D MoS₂ were alike topographically in the sense of possessing deformation streaks along the sliding direction, the depths of furrows on the steel ball worn surfaces were diverse. As shown in Figure 5a,b, the morphologies of steel ball worn surfaces lubricated by CSCG were coarser, and the furrows were deeper and more concentrated. These surface characteristics ulteriorly certified the severe adhesive wear that occurred on the worn surfaces of the steel ball. As a comparison, the furrows on the morphologies of steel ball worn surfaces lubricated by CSCG + 0.6 wt.% 2D MoS₂ were shallower. Compared with CSCG, the surface roughness and average wear depths of CSCG + 0.6 wt.% 2D MoS₂ were 0.54 and 5.41 μm, reducing by 14.3% and 59.4%, respectively. It was supposed that the influence of 2D MoS₂ mitigated adhesion.

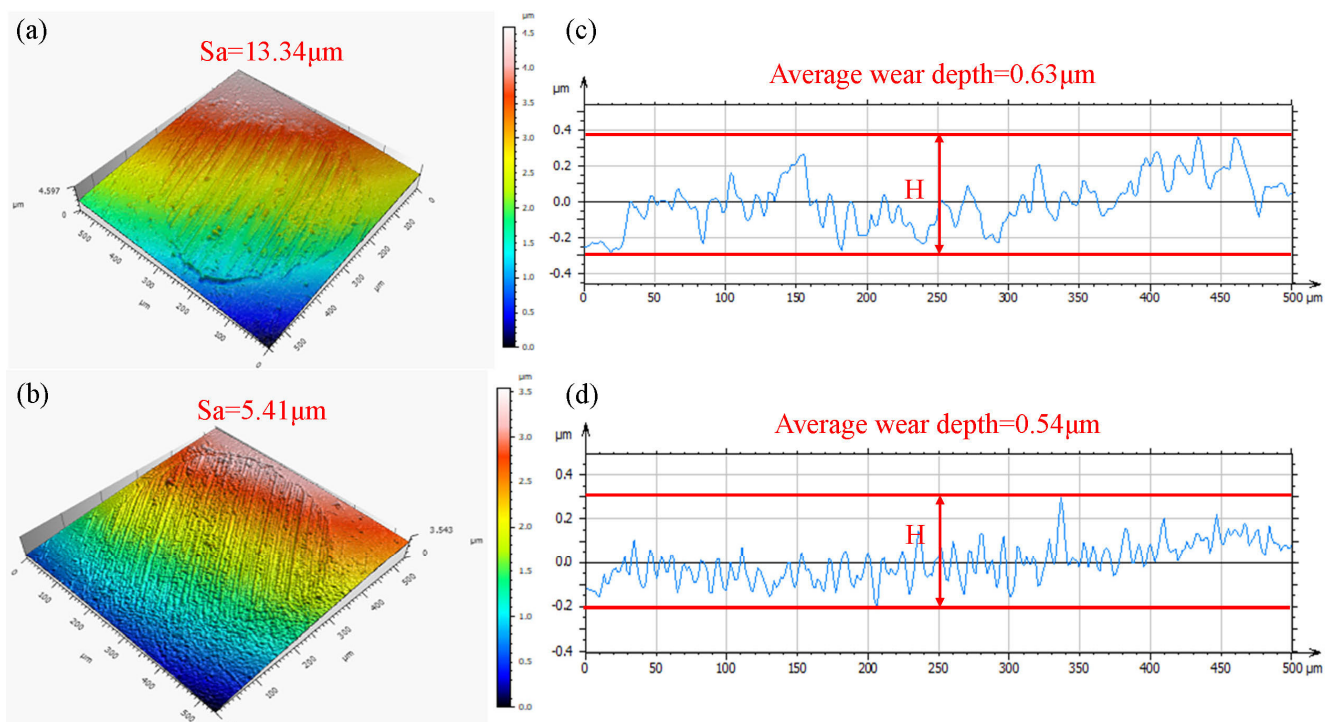


Figure 5. 3D morphology and average depth of steel ball wear scar surface, (a,c) lubricated by CSCG, (b,d) lubricated by CSCG + 0.6 wt.% 2D MoS₂.

3.3. Wear Morphology Analysis

The transferred 2D MoS₂ film was confirmed by Raman spectra as demonstrated in Figure 6. There were some dark spots distinctly arising on the wear scar of the steel ball. Evident E_{2g}¹ and A_{1g} bonds could be seen from the correlating Raman spectra, which could confirm the existence of 2D MoS₂ film compared to the Raman spectra of the wear scar without 2D MoS₂. However, with the addition of 2D MoS₂ to the CSCG, the 2D MoS₂ displayed increased defects during the four-ball test as witness to the increase of A_{1g} bond intensity ($I_{A_{1g}}/I_{E_{2g}^1}$) from 1.11 of 2D MoS₂ before rotating sliding to 1.13 after rotating sliding. Combined with the Raman spectra, the above-mentioned four-ball tests depicted that the lamellar 2D MoS₂ are crushed into the contact area between the four steel balls. The 2D MoS₂ were adsorbed physically on the surface of the steel ball and generated an adsorption film to hold direct contact between the steel balls and decrease the friction influence on the rubbing pairs of the substrate.

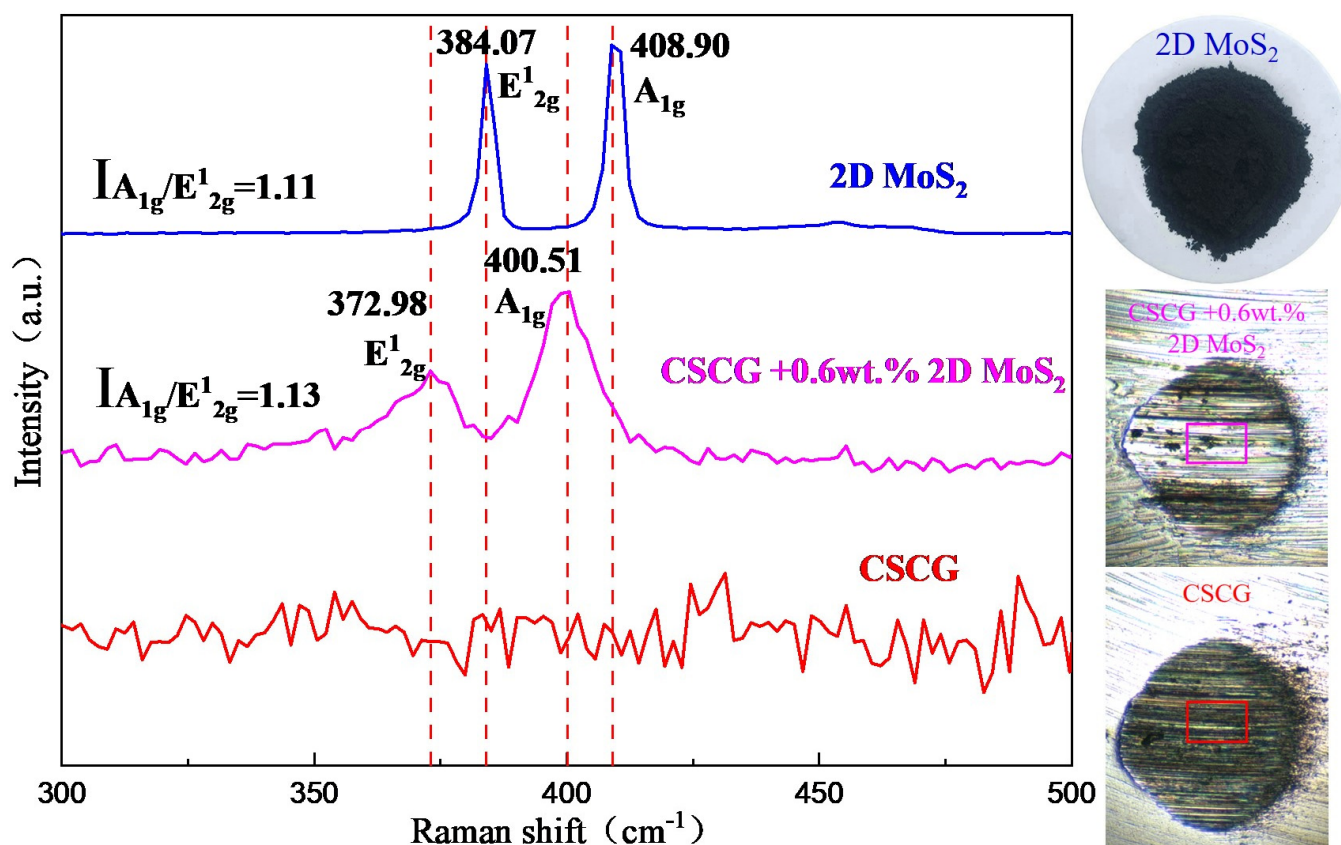


Figure 6. Raman spectra and optical micrographs of 2D MoS₂, worn surface on steel ball lubricated by CSCG, CSCG + 0.6 wt.% 2D MoS₂.

For purpose of analyzing the composition of the tribo-film, the surface distribution of typical elements was explored. As shown in Figure 7, there is prominent debris on the wear surface. In addition to the base element iron (Fe), a large amount of calcium (Ca), carbon (C), oxygen (O), and sulfur (S) elements were gathered on the wear surface. C elements originated from the base oil PAO40, and Ca and S elements originated from the sulfonate calcium and complex calcium soap of CSCG. However, the oxygen (O) elements corresponded to the oxidation arising from friction heat. Without the participation of 2D MoS₂, the severe friction resulted from direct adhesion between the steel balls and gave rise to a great deal of friction heat, which brought about oxidation on the surface, the emergence of oxide film dramatically decreased the surface energy of rubbing the surface, and diminishes the COF to some extent.

According to the EDS spectrum of the wear surface lubricated by CSCG + 0.6 wt.% 2D MoS₂ in Figure 8, the surface of the wear scar is visibly smooth, and the furrow becomes flat. With the participation of 2D MoS₂, the chemical constituents of the lubricated steel ball wear scar mostly consisted of calcium (Ca), carbon (C), oxygen (O), iron (Fe), sulfur (S), and molybdenum (Mo). It is worth noting that a small quantity of Mo elements also appeared on the wear surface, which came from the 2D MoS₂. At the same time, the appearance of Mo on the wear surface lubricated by CSCG + 0.6 wt.% 2D MoS₂ resulted in a new film generating mechanism and structure.

Exploring the correlation between the contact surface of rubbing pairs and 2D MoS₂ during the period of the four-ball test is of great necessity. To validate the friction-reducing and anti-wear mechanism of 2D MoS₂, an XPS spectrum of characteristic elements on the wear scars was utilized to detect their chemical states. Figure 9 demonstrates that a survey spectra of the worn surface occurred on the steel ball lubricated by the CSCG. The XPS spectrum of wear surface lubricated by the CSCG explicitly exhibited the presence of S 2p,

C 1s, Ca 2p, O 1s, and Fe 2p peaks at 168.7 eV, 286.6 eV, 531.5 eV, 712.1 eV, and 348.1 eV, respectively. The C 1s peaks appear at 284.8 eV, 286.3 eV, and 286.6 eV, which suggests the existence of complicated carbon oxide. Two Ca 2p peaks located at 348.1 eV and 351.4 eV are attributed to CaSO_4 or CaCO_3 or CaO , which confirmed the appearance of CaO , CaSO_4 , and CaCO_3 [28]. The Fe 2p peaks are located at around 712.1 eV and 709.5 eV due to the formation of Fe_2O_3 . The O 1s peaks at 531.5 eV elucidate the formation of oxidative products on the worn surfaces. The S 2p peaks at about 161.5 eV verified the existence of MoS_2 on the worn surface. Meanwhile, the S 2p peaks at about 168.7 eV, illuminating that the tribo-chemical reaction was concerned with the sulfides and sulfates, such as FeS and FeSO_4 . This result proves that the Ca element, particularly CaCO_3 and CaSO_4 , makes an important contribution to the protective mechanism of the CSCG. Based on the results of the XPS, it can be inferred that a tribo-chemical film came into being on the contact surface during the period of friction process, which is composed of Fe_2O_3 , FeSO_4 , CaCO_3 , and CaO .

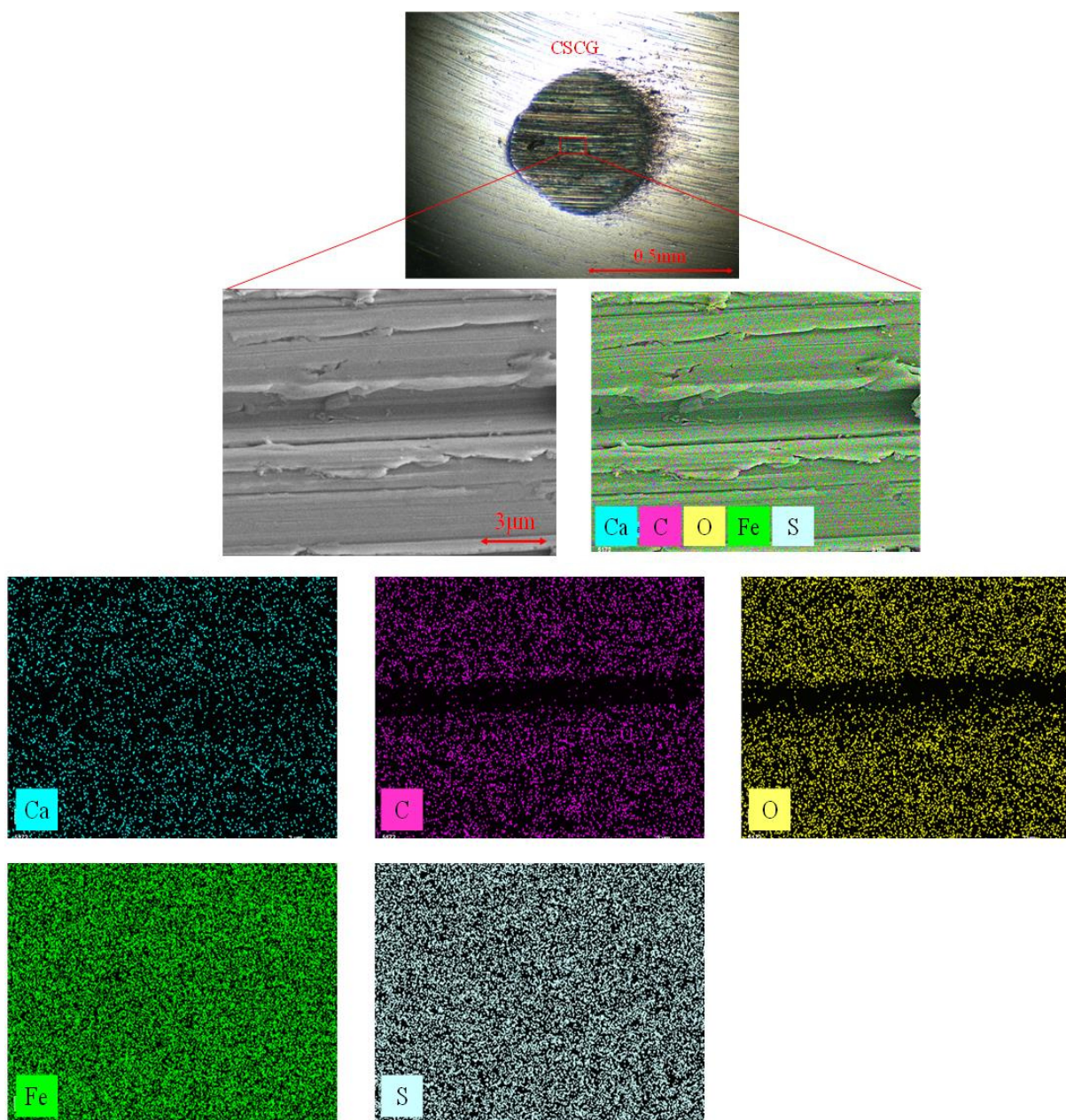


Figure 7. SEM images and EDS mapping of steel ball wear scar lubricated by CSCG.

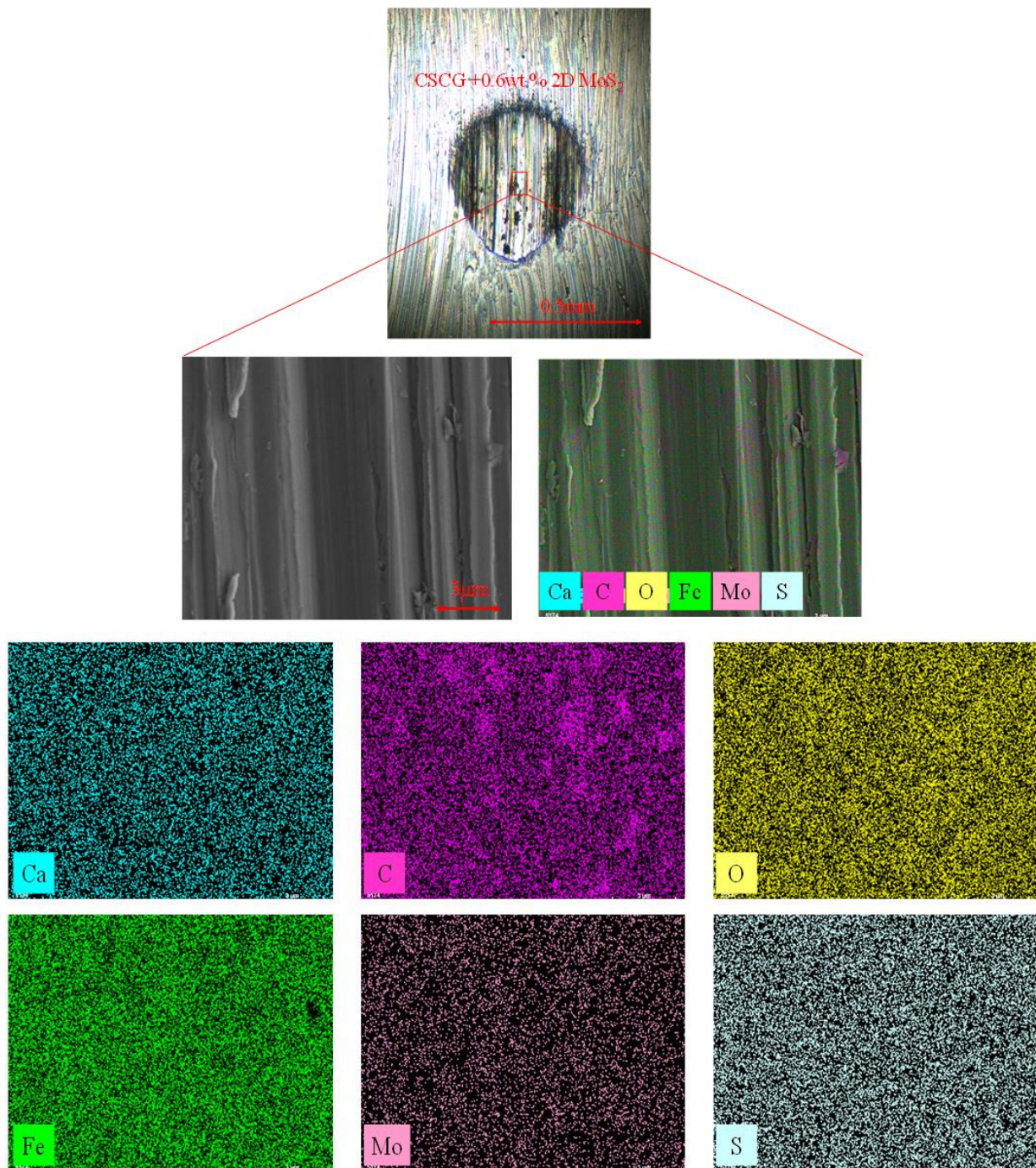


Figure 8. SEM images and EDS mapping of steel ball wear scar lubricated by CSCG + 0.6 wt.% 2D MoS₂.

Figure 10 provides the XPS spectra of the worn surface that appeared on the steel ball lubricated by the CSCG + 0.6 wt.% 2D MoS₂. The XPS spectrum of wear surface lubricated by the CSCG+ 0.6 wt.% 2D MoS₂ clearly showed the presence of S 2p, Mo 3d, C 1s, Ca 2p, O 1s, and Fe 2p peaks at 168.7 eV, 232.5 eV, 286.6eV, 531.5 eV, 712.1 eV, and 348.1 eV, respectively. The peak of the C 1s spectrum at 286.6 eV, 286.3 eV, and 284.8 eV indicates the presence of complicated carbon oxides. The Ca 2p peak of CSCG came out at 348.1 eV and 351.7 eV, attributed to CaCO₃ and CaO, separately, which are the products of physical adsorption and tribo-chemical reactions of CSCG thickener on the contact surface. The characteristic peaks of Fe 2p at 713.0 eV and 710.2 eV depict the appearance of Fe₂O₃. After

adding 2D MoS₂ to the CSCG, the Mo 3d peaks at 228.8 eV and 232.5 eV corresponded to MoS₂ and MoO₃ [29], respectively. The O 1s peaks at 532.1 eV are owing to the presence of complicated oxide on the worn surface. The S 2p peaks at about 168.7 eV, illuminating that tribo-chemical reaction was concerned with the sulfides and sulfates, such as FeS and FeSO₄. The S 2p peaks at about 162.3 eV, verifying the existence of MoS₂ on the worn surface [30]. In terms of the above analysis, we can draw the conclusion that a tribo-chemical reaction took place during the period of the sliding process and a protective film consisting of Fe₂O₃, FeSO₄, CaCO₃, CaO, and MoO₃ was formed.

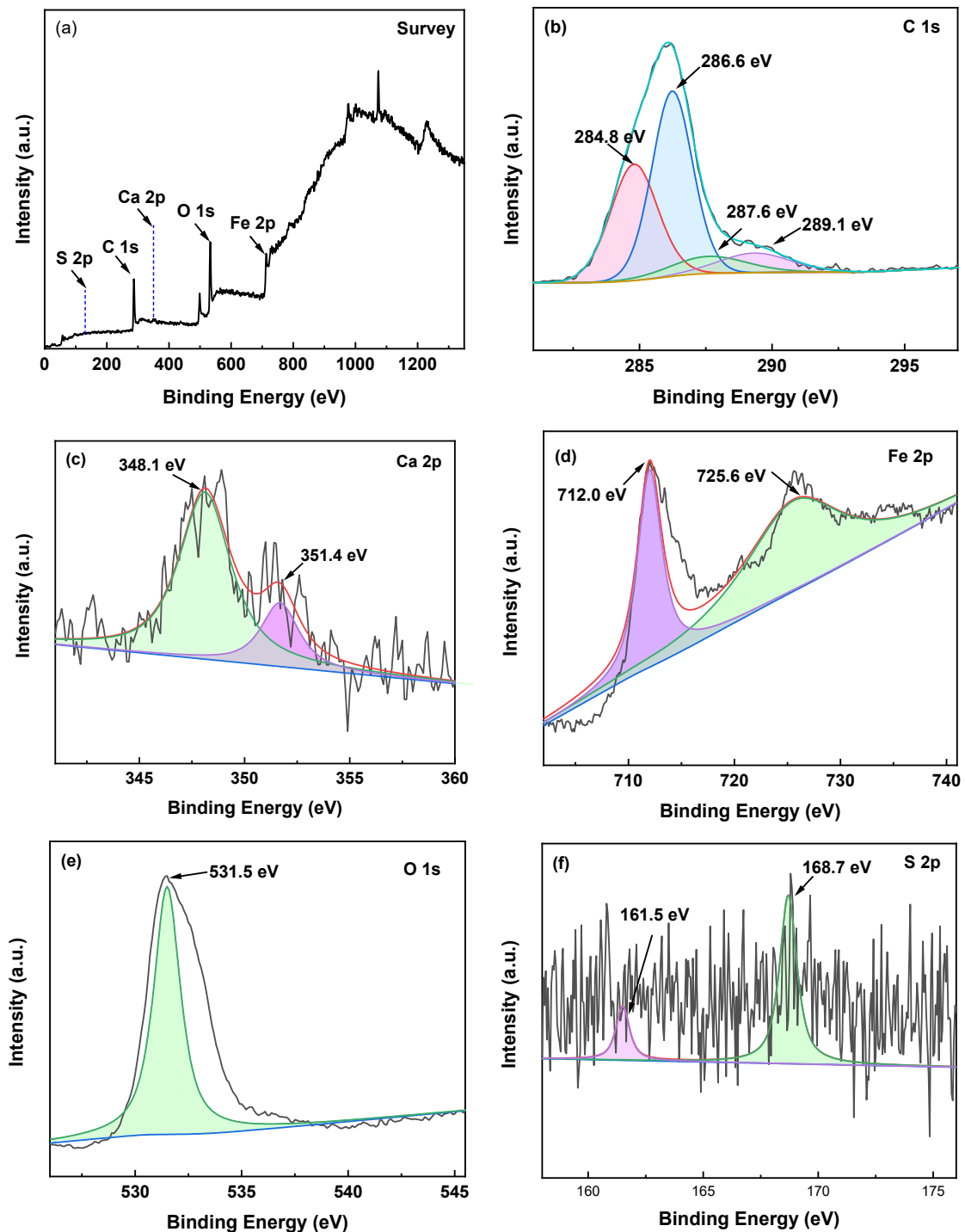


Figure 9. XPS spectrum of steel ball wear spot surface lubricated by CSCG, (a) XPS survey spectra, (b) C 1s, (c) Fe 2p, (d) O 1s, (e) Ca 2p, (f) S 2p.

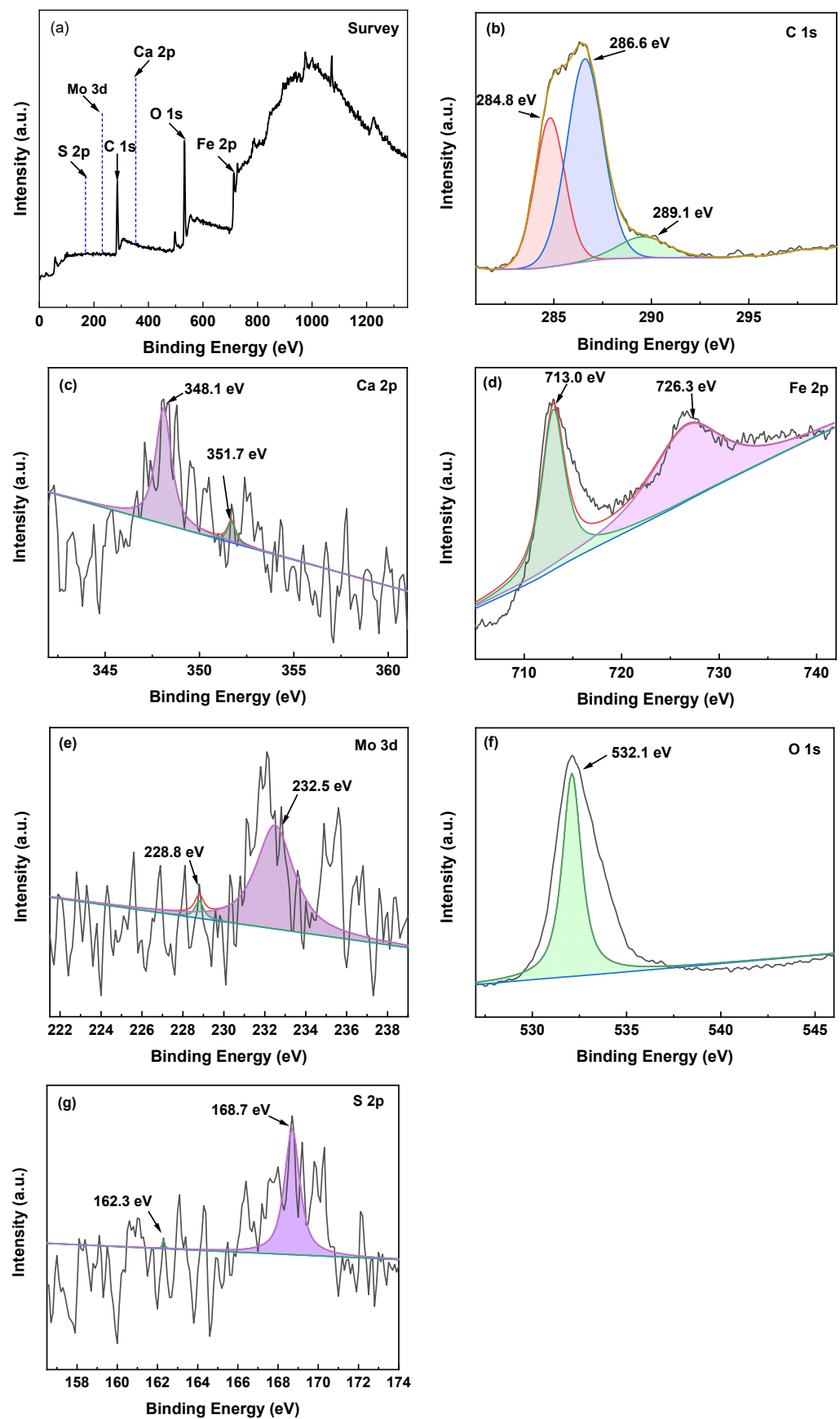


Figure 10. XPS spectrum of steel ball wear spot surface lubricated by CSCG + 0.6 wt.% 2D MoS₂. (a) XPS survey spectra, (b) C 1s, (c) Ca 2p, (d) Fe 2p, (e) Mo 3d, (f) O 1s, (g) S 2p.

3.4. Lubrication Mechanism

On the basis of the aforementioned results, the lubrication mechanisms can be generalized for the subsequent two aspects: the interlayer slipping of physical transferred film and the formation of tribo-chemical film, which are schematically described in Figure 11. The 2D MoS₂ could readily pass into the rubbing contact attributing to its sheet shape and small size. At the initial stage of friction tests, the 2D MoS₂ formed a physical transferred film between the GCr15 steel balls, as illustrated in Figure 11a. When two mutually contacting surfaces rub up against each other under normal force, the 2D MoS₂ in the contact area is prone to normal pressure. The relative motion of the two mutually contacting surfaces provides a shear stress to 2D MoS₂. As a consequence, the easily shearing characteristic of 2D MoS₂ forms a sliding system with the friction pair. In comparison with rigid contact, the friction force in the sliding system is much smaller, resulting in high-efficiency lubrication. The physical transferred film cracks as the continual sliding proceeds. A great deal of heat is produced at this time and it stimulates a tribo-chemical reaction between the lubricant and substrate. A new tribo-chemical film formed and gradually replaces the physical transferred film, which mainly consists of Fe₂O₃, FeSO₄, CaCO₃, CaO, and MoO₃. This film is not only coming into being on the localized contact surfaces but also in the matrix of the substrate, which enhances the lubrication performance considerably.

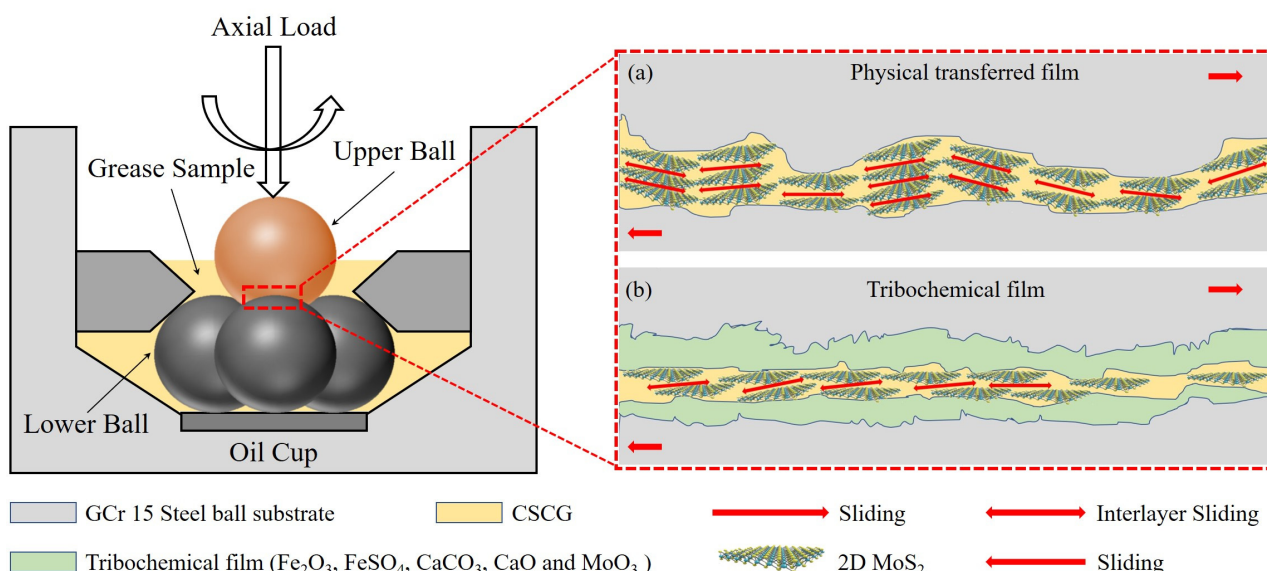


Figure 11. Schematic diagrams of lubrication mechanism for CSCG enhanced with 2D MoS₂: (a) the interlayer slipping of physical transferred film, (b) the formation of tribo-chemical film.

4. Conclusions

A 2D MoS₂ with a narrow lateral size and thickness distributions exhibited outstanding friction-reducing and anti-wear properties, and could also markedly enhance the lubrication performance of CSCG, possessing excellent ability in reducing the average friction coefficient (AFC), wear scar diameter (WSD), surface roughness, and average wear depth during the four-ball tests. The lubrication mechanisms are shown as follows. (1) The 2D MoS₂ was adsorbed on the surface of the steel ball and formed a physical transferred film to prevent direct contact between the steel balls and decrease the friction influence of the rubbing pairs on the substrate. (2) A new tribo-chemical film formed and gradually replaced the physical transferred film, which mainly consisted of Fe₂O₃, FeSO₄, CaCO₃, CaO, and MoO₃, which improves the lubrication performance considerably. In extreme working conditions, such as high temperature, high load, and high speed, the physical transferred film is broken off easily and the tribo-chemical film forms subsequently, which plays a predominant role in lubrication between the steel balls.

Author Contributions: Investigation, S.X., X.L., Q.Z. and P.M.; resources, S.X. and Q.Z.; methodology and validation, S.X., X.Y. and H.X.; visualization and formal analysis, S.X., P.L. and P.S.; supervision, S.X., Q.Z., W.Y. and Y.H.; writing—original draft preparation, S.X., X.L., Q.Z. and P.M.; writing—review and editing, S.X., X.L., Q.Z., X.Y., H.X., P.L., P.S., W.Y. and Y.H. All authors have read and agreed to the published version of the manuscript.

Funding: This research was funded by Science and Technology Research Program of Chongqing Municipal Education Commission, grant number KJZD-K202212905 and Natural Science Foundation of Chongqing, grant number cstc2019jcyj-msxmX0453.

Data Availability Statement: Data are contained within the article.

Conflicts of Interest: Author Hui Xu was employed by the Shandong Honsing Chemical Co. Ltd. The remaining authors declare that the research was conducted in the absence of any commercial or financial relationships that could be construed as a potential conflict of interest. The potential conflict of interest was reported by the authors.

References

1. Dwaine, M. Novel Lithium Free Thickener System: Performance Profile, Characteristics and Target Applications. *NLGI Spokesm.* **2022**, *86*, 8–16.
2. Adaikkappan, M.; Sathiyamoorthy, N. Modeling, State of Charge Estimation, and Charging of Lithium-Ion Battery in Electric Vehicle: A Review. *Int. J. Energ. Res.* **2022**, *46*, 2141–2165. [[CrossRef](#)]
3. Ren, G.; Zhang, P.; Li, W.; Fan, X.; Zhang, L.; Li, H.; Zhu, M. Probing the Synergy of Blended Lithium Complex Soap and Calcium Sulfonate Towards Good Lubrication and Anti-Corrosion Performance. *Tribol. Lett.* **2020**, *68*, 99. [[CrossRef](#)]
4. Wang, W.; Qian, S.; Gong, L.; Ni, Z.; Ren, H. Effects of Carbon Nano Onions on the Tribological Performance of Food-grade Calcium Sulfonate Complex Grease. *Lubr. Sci.* **2021**, *33*, 460–470. [[CrossRef](#)]
5. Wu, C.; Liu, Z.; Ni, J.; Yang, K.; Yang, H.; Li, X. Improved Tribological and Bearing Vibration Performance of Calcium Sulfonate Complex Grease Dispersed with MoS₂ and Oxide Nanoparticles. *Proc. Inst. Mech. Eng. Part C J. Mech. Eng. Sci.* **2023**, *237*, 1941–1955. [[CrossRef](#)]
6. Wang, B.; Qiu, F.; Barber, G.C.; Zou, Q.; Wang, J.; Guo, S.; Yuan, Y.; Jiang, Q. Role of Nano-Sized Materials as Lubricant Additives in Friction and Wear Reduction: A Review. *Wear* **2022**, *490–491*, 204206. [[CrossRef](#)]
7. Guan, Z.; Zhang, P.; Florian, V.; Wu, Z.; Zeng, D.; Liu, J.; Wang, B.; Tu, X.; Li, S.; Li, W. Preparation and Tribological Behaviors of Magnesium Silicate Hydroxide-MoS₂ Nanoparticles as Lubricant Additive. *Wear* **2022**, *492–493*, 204237. [[CrossRef](#)]
8. Mousavi, S.B.; Heris, S.Z.; Estellé, P. Experimental Comparison between ZnO and MoS₂ Nanoparticles as Additives on Performance of Diesel Oil-Based Nano Lubricant. *Sci. Rep.* **2020**, *10*, 5813. [[CrossRef](#)]
9. Fayaz, S.D.; Wani, M. Insights into the Tribological Behavior of IF-WS₂ Nanoparticle Reinforced Mild Extreme Pressure Lubrication for Coated Chromium/Bulk Grey Cast Iron Interface. *Proc. Inst. Mech. Eng. Part J J. Eng. Tribol.* **2021**, *235*, 1478–1494. [[CrossRef](#)]
10. Zhao, Z.; Fan, X.; Li, Y.; Zeng, Z.; Wei, X.; Lin, K.; Zhu, M. Well-Dispersed Graphene toward Robust Lubrication via Reorganization of Sliding Interface. *J. Ind. Eng. Chem.* **2023**, *119*, 619–632. [[CrossRef](#)]
11. Larsson, E.; Westbroek, R.; Leckner, J.; Jacobson, S.; Rudolphi, A.K. Grease-Lubricated Tribological Contacts—Influence of Graphite, Graphene Oxide and Reduced Graphene Oxide as Lubricating Additives in Lithium Complex (LiX)- and Polypropylene (PP)-Thickened Greases. *Wear* **2021**, *486–487*, 204107. [[CrossRef](#)]
12. Gan, C.; Liang, T.; Li, X.; Li, W.; Li, H.; Fan, X.; Zhu, M. Ultra-Dispersive Monolayer Graphene Oxide as Water-Based Lubricant Additive: Preparation, Characterization and Lubricating Mechanisms. *Tribol. Int.* **2021**, *155*, 106768. [[CrossRef](#)]
13. Liang, X.; Ji, H. Tribological Properties of Lubricating Grease Additives Made of Silica and Silicon Carbide Nanomaterials. *Integr. Ferroelectr.* **2022**, *225*, 212–224. [[CrossRef](#)]
14. Buyanovskii, I.A.; Bolshakov, A.N.; Levchenko, V.A. The Effect of Orienting Carbon Coatings Alloyed with Carbide-Forming Elements on the Antifriction Properties of Lubricants. *J. Frict. Wear* **2018**, *39*, 371–375. [[CrossRef](#)]
15. Yang, W.; Geng, Z.; Li, Y.; Liu, X.; Tian, X.; Wang, S.; Wu, N.; Wang, Y.; Xu, R.; Yang, F.; et al. Facile Synthesis of Lipophilic Alkylated Boron Nitride Nanosheets as Lubricating Oil Additive to Greatly Enhance the Friction and Heat-Conducting Properties. *Tribol. Int.* **2022**, *173*, 107655. [[CrossRef](#)]
16. Xu, Y.; Yu, J.; Dong, Y.; You, T.; Hu, X. Boundary Lubricating Properties of Black Phosphorus Nanosheets in Polyalphaolefin Oil. *J. Tribol.* **2019**, *141*, 072101. [[CrossRef](#)]
17. Tang, G.; Su, F.; Xu, X.; Chu, P.K. 2D Black Phosphorus Dotted with Silver Nanoparticles: An Excellent Lubricant Additive for Tribological Applications. *Chem. Eng. J.* **2020**, *392*, 123631. [[CrossRef](#)]
18. Wang, W.; Dong, S.; Gao, Y.; Zhang, G.; Wang, K. Tribological Behaviours of Black Phosphorus/MoS₂ Composites as Water-based Lubrication Additives. *Lubr. Sci.* **2021**, *33*, 404–416. [[CrossRef](#)]
19. Yu, T.; Xu, S.; Wu, Z.; Wang, D. 2D SiP Nanoflakes as New High-Performance Lubricant Additive for Steel/Steel Sliding Contact. *Tribol. Int.* **2022**, *169*, 107467. [[CrossRef](#)]

20. Zhao, J.; Gao, T.; Li, Y.; He, Y.; Shi, Y. Two-Dimensional (2D) Graphene Nanosheets as Advanced Lubricant Additives: A Critical Review and Prospect. *Mater. Today Commun.* **2021**, *29*, 102755. [[CrossRef](#)]
21. Baig, N. Two-Dimensional Nanomaterials: A Critical Review of Recent Progress, Properties, Applications, and Future Directions. *Compos. Part A Appl. Sci.* **2023**, *165*, 107362. [[CrossRef](#)]
22. Patel, G.; Pillai, V.; Vora, M. Liquid Phase Exfoliation of Two-Dimensional Materials for Sensors and Photocatalysis-A Review. *J. Nanosci. Nanotechnol.* **2019**, *19*, 5054–5073. [[CrossRef](#)] [[PubMed](#)]
23. Li, F.; Sun, S.-K.; Chen, Y.; Naka, T.; Hashishin, T.; Maruyama, J.; Abe, H. Bottom-up Synthesis of 2D Layered High-Entropy Transition Metal Hydroxides. *Nanoscale Adv.* **2022**, *4*, 2468–2478. [[CrossRef](#)] [[PubMed](#)]
24. Noreen, S.; Tahir, M.B.; Hussain, A.; Nawaz, T.; Rehman, J.U.; Dahshan, A.; Alzaid, M.; Alrobei, H. Emerging 2D-Nanostructured Materials for Electrochemical and Sensing Application-A Review. *Int. J. Hydrogen Energy* **2022**, *47*, 1371–1389. [[CrossRef](#)]
25. Chen, T.; Kaur, H.; McCrystall, M.; Tian, R.; Roy, A.; Smith, R.; Horvath, D.V.; Maughan, J.; Konkana, B.; Venkatesan, M.; et al. Liquid Phase Exfoliation of Nonlayered Non-van Der Waals Iron Trifluoride (FeF₃) into 2D-Platelets for High-Capacity Lithium Storing Cathodes. *Flatchem* **2022**, *33*, 100360. [[CrossRef](#)]
26. Lu, P.; Xiang, S.; Xu, S.; Chen, H.; Wang, H.; Wang, J.; Zhang, G. Tribological study on preparation of two-dimensional MoS₂ as grease additive by ultrasonic liquid phase stripping. *J. Mater. Eng.* **2023**, *51*, 160–168.
27. Gupta, N.; Tandon, N.; Pandey, R.K.; Vidyasagar, K.E.C.; Kalyanasundaram, D. Tribodynamic Studies of Textured Gearsets Lubricated with Fresh and MoS₂ Blended Greases. *Tribol. Int.* **2022**, *165*, 107247. [[CrossRef](#)]
28. Zhou, C.; Ren, G.; Fan, X.; Lv, Y. Probing the Effect of Thickener Microstructure on Rheological and Tribological Properties of Grease. *J. Ind. Eng. Chem.* **2022**, *111*, 51–63. [[CrossRef](#)]
29. Jiang, H.; Hou, X.; Ma, Y.; Su, D.; Qian, Y.; Ahmed Ali, M.K.; Dearn, K.D. The Tribological Performance Evaluation of Steel-Steel Contact Surface Lubricated by Polyalphaolefins Containing Surfactant-Modified Hybrid MoS₂/h-BN Nano-Additives. *Wear* **2022**, *504–505*, 204426. [[CrossRef](#)]
30. Fan, X.; Li, W.; Li, H.; Zhu, M.; Xia, Y.; Wang, J. Probing the Effect of Thickener on Tribological Properties of Lubricating Greases. *Tribol. Int.* **2018**, *118*, 128–139. [[CrossRef](#)]

Disclaimer/Publisher's Note: The statements, opinions and data contained in all publications are solely those of the individual author(s) and contributor(s) and not of MDPI and/or the editor(s). MDPI and/or the editor(s) disclaim responsibility for any injury to people or property resulting from any ideas, methods, instructions or products referred to in the content.